The Journal of Clinical Endocrinology & Metabolism, 2020, Vol. XX, No. XX, 1–13
doi:10.1210/clinem/dgaa819
Clinical Research Article

Clinical Research Article

Germline *DLST* Variants Promote Epigenetic Modifications in Pheochromocytoma-Paraganglioma

Alexandre Buffet,*[1,2] Juan Zhang,*[3] Heggert Rebel,[3] Eleonora P. M. Corssmit,[4] Jeroen C. Jansen,[5] Erik F. Hensen,[5] Judith V. M. G. Bovée,[6] Aurélien Morini,[7] Anne-Paule Gimenez-Roqueplo,[1,2] Frederik J. Hes,[8] Peter Devilee,[3,6] Judith Favier,[2] and Jean-Pierre Bayley**[3]**

[1]Université de Paris, PARCC, INSERM, Equipe Labellisée par la Ligue contre le Cancer, F-75015 Paris, France; [2]Genetic department, Adrenal Referral Center, Assistance Publique-Hôpitaux de Paris (AP-HP), Hôpital Européen Georges Pompidou, F-75015 Paris, France; [3]Department of Human Genetics, Leiden University Medical Center, 2300 RC, Leiden, The Netherlands; [4]Department of Endocrinology and Metabolic Diseases, Leiden University Medical Center, 2300 RC, Leiden, The Netherlands; [5]Department of Otorhinolaryngology, Leiden University Medical Center, 2300 RC, Leiden, The Netherlands; [6]Department of Pathology, Leiden University Medical Center, 2300 RC, Leiden, The Netherlands; [7]Assistance Publique-Hôpitaux de Paris (AP-HP), Hôpital Européen Georges Pompidou, Département d'anatomo-pathologie, F-75015 Paris, France; and [8]Department of Clinical Genetics, Leiden University Medical Center, 2300 RC, Leiden, The Netherlands

ORCiD numbers: 0000-0002-4742-2708 (A. Buffet); 0000-0001-9836-9137 (E. P. M. Corssmit); 0000-0002-4393-7421 (E. F. Hensen); 0000-0003-1155-0481 (J. V. M. G. Bovée); 0000-0002-4816-670X (A.-P. Gimenez-Roqueplo); 0000-0002-8023-2009 (P. Devilee); 0000-0001-8190-5853 (J. Favier); 0000-0002-8288-0050 (J.-P. Bayley).

*Joint first authors
**Joint senior authors

Abbreviations: 5hmC, 5-hydroxymethylcytosine; 5mC, 5-methyl cytosine;A_{450}, absorbance at 450 nm;DLST, dihydrolipoamide S-succinyltransferase;DMEM, Dulbecco's Modified Eagle Medium; ELISA, enzyme-linked immunosorbent assay; FFPE, formalin-fixed, paraffin-embedded;HIF, hypoxia-inducible factor;NADH, nicotinamide adenine dinucleotide;OGDH, oxoglutarate dehydrogenase enzyme complex;PCC, pheochromocytoma;PCR, polymerase chain reaction;PGL, paraganglioma;PPGL, pheochromocytoma/paraganglioma;TCA, tricarboxylic acid;TET, ten-eleven-translocation;WT, wild-type.

Received: 25 March 2020; Editorial Decision: 31 October 2020; First Published Online: 12 November 2020; Corrected and Typeset: 15 December 2020.

Abstract

Context

Pheochromocytomas and paragangliomas (PPGLs) are neuroendocrine tumors in which altered central metabolism appears to be a major driver of tumorigenesis, and many PPGL genes encode proteins involved in the tricarboxylic acid (TCA) cycle.

Objective/design

While about 40% of PPGL cases carry a variant in a known gene, many cases remain unexplained. In patients with unexplained PPGL showing clear evidence of a familial burden or multiple tumors, we aimed to identify causative factors using genetic analysis

ISSN Print 0021-972X ISSN Online 1945-7197
Printed in USA

of patient DNA and functional analyses of identified DNA variants in patient tumor material and engineered cell lines.

Patients and Setting

Patients with a likely familial cancer burden of pheochromocytomas and/or paragangliomas and under investigation in a clinical genetic and clinical research setting in university hospitals.

Results

While investigating unexplained PPGL cases, we identified a novel variant, c.1151C>T, p.(Pro384Leu), in exon 14 of the gene encoding dihydrolipoamide S-succinyltransferase (*DLST*), a component of the multi-enzyme complex 2-oxoglutarate dehydrogenase. Targeted sequence analysis of further unexplained cases identified a patient carrying a tumor with compound heterozygous variants in *DLST*, consisting of a germline variant, c.1121G>A, p.(Gly374Glu), together with a somatic missense variant identified in tumor DNA, c.1147A>G, p.(Thr383Ala), both located in exon 14. Using a range of in silico and functional assays we show that these variants are predicted to be pathogenic, profoundly impact enzyme activity, and result in DNA hypermethylation.

Conclusions

The identification and functional analysis of these *DLST* variants further validates *DLST* as an additional PPGL gene involved in the TCA cycle.

Key Words: Paraganglioma, pheochromocytoma, dihydrolipoamide S-succinyltransferase, *DLST*, 2-oxoglutarate dehydrogenase, methylation

Introduction

Paragangliomas (PGLs) are neuroendocrine tumors that may arise in either the sympathetic or parasympathetic ganglia. Parasympathetic PGLs occur most commonly in the head and neck region (carotid body, jugular paraganglia, and tympanic paraganglia), are generally benign and are rarely associated with the secretion of catecholamines. PGLs arising from the sympathetic ganglia are mostly found in the abdomen and thorax, are frequently detected due to endocrine-related hypertension associated with excess secretion of catecholamines and are associated with a higher risk of malignancy. Paragangliomas that arise in the chromaffin cells of the adrenal medulla, commonly referred to as pheochromocytomas (PCCs), are usually benign and are also frequently associated with hypertension due to excessive catecholamine secretion (1). Collectively, these tumors are often referred to as pheochromocytomas and paragangliomas (PPGLs).

PPGLs are associated with a heterogeneous collection of both germline and somatic variants found in up to 19 genes to date, although about half of all candidate PGL genes still have ill-defined pathogenicity (2, 3). PGL-associated genes belong to a wide range of functional categories that include kinase receptors (*RET*), regulators of signaling (*NF1*, *HRAS*), hypoxia-related factors (*VHL*, *EPAS1* [HIF2A]), tricarboxylic acid cycle (TCA) enzymes involved in energy metabolism (*SDHA*, *SDHB*, *SDHC*, *SDHD*, *SDHAF2*, *FH*, *MDH2*, *IDH1*, *IDH2*), members of the malate-aspartate shuttle (*SLC25A11*, *GOT2*), an endosomal signaling factor (*TMEM127*), and a transcription factor (*MAX*). Nonetheless, most PPGLs can be attributed to variants in genes involved in metabolism, currently including *SDHA*, *SDHB*, *SDHC*, *SDHD*, *SDHAF2*, *FH*, *MDH2*, *IDH1*, *IDH2*, *GOT2*, and *SLC25A11*.

Although the mechanisms by which mutations in metabolic enzymes promote tumor formation are not yet fully understood, inactivation of *SDH*, *FH*, and *IDH1/2* leads to the accumulation of so-called "oncometabolites," intermediary metabolites such as succinate, fumarate, and 2-hydroxyglutarate that are known to inhibit dioxygenases (4-6), a large group of enzymes of diverse function. Perhaps the most important of these are the hypoxia-inducible factor (HIF) prolyl hydroxylases, which when disturbed cause HIF activation under normoxia (5), and other dioxygenases including histone demethylases and the TET (ten-eleven translocation) family of 5-methylcytosine (5mC) hydroxylases (7-9) that result in altered patterns of histone methylation or hypermethylation known as a CpG-island methylator-phenotype (CIMP) (10).

In addition, PPGL tumors can be classified into 2 major clusters in terms of gene expression patterns (11), together with several minor clusters (12). Cluster 1 tumors, which include tumors carrying variants in the succinate dehydrogenase (*SDH*) genes and *VHL*, were found to differ markedly from cluster 2 (including *RET* and *NF1*) pheochromocytomas, with cluster 1 tumors characterized

by angiogenesis, hypoxia, extracellular matrix, and suppression of oxidoreductase enzymes activity, whereas cluster 2 tumors show gene expression patterns related to translation initiation, protein synthesis, and kinase signaling.

In this study of unexplained PPGL cases with a suspected genetic burden, we identified and functionally investigated 3 likely pathogenic variants of *DLST*, the gene that encodes dihydrolipoamide S-succinyltransferase, the E2 subunit of the 2-oxoglutarate dehydrogenase enzyme complex (OGDH), the rate-limiting enzyme in the TCA cycle. This enzyme complex catalyzes the transfer of the succinyl group from a S-succinyldihydrolipoyl moiety to coenzyme A as part of the overall conversion of 2-oxoglutarate to succinyl-CoA and CO_2 by OGDH. Variants in *DLST* were recently reported to play a role in PPGL (13).

Material and Methods

DNA analysis

Five patients were initially selected for exome sequencing based on the incidence of multiple tumors or a family history, together with negative results for a standard panel of PPGL-related genes, including 5 *SDH* genes, *VHL*, *RET*, *TMEM127*, and *MAX*. Paired-end sequencing was carried out by a service provider (Macrogen, Seoul, Korea) using peripheral blood lymphocyte DNA. An NGS sequencing library was prepared using the SureSelect^{XT} Library Prep Kit (Illumina) following the SureSelectXT Target Enrichment System protocol version B.2, with sequencing on a HiSeq 4000 machine (Illumina). Sequence reads were then aligned to the reference genome and variants called.

One of these patients was found to carry a c.1151C>T, p.(Pro384Leu) variant in *DLST*, which was subsequently confirmed by Sanger sequencing of exon 14. Analysis of other unexplained samples was then conducted based on standard polymerase chain reaction (PCR) and Sanger sequencing protocols using the *DLST* exon 14 forward primer 3389 (5′-TGTAAAACGACGGCCAGT-3′) and reverse primer 3377 (5′-CAGGAAACAGCTATGACC-3′). We analyzed DNAs from 169 patients with a PPGL available through the COMETE and PGL.NET networks (Table 1). All patients had a phenotype consistent with hereditary PPGL (early onset, multiple or family history of PPGL) but without a germline mutation in any of the known PPGL susceptibility genes. Of these patients, 90% had a benign PPGL and 10% a metastatic PPGL, while 27% had multiple PPGLs. The procedures used for PPGL diagnosis were in accordance with international guidelines (14, 15). Each patient gave written informed consent for genetic analyses.

Patient tissue samples

Formalin-fixed paraffin-embedded (FFPE) pheochromocytoma tissue samples (from patient 1—see below) were retrieved from the archives of the Department of Pathology, Leiden University Medical Center. The histological appearance of all samples was reviewed by an experienced pathologist (JVMGB) and the diagnosis was supported by routine S-100, chromogranin A, and SDHB immunohistochemical staining. All samples were handled according to the Federation of Dutch Medical Scientific Societies (www.federa.org) code of proper secondary use of human material, approved by the Dutch Society of Pathology and in accordance with procedures agreed upon with the LUMC ethical board. Patient 1 provided written informed consent.

Tissue microarrays generated in the Departments of Pathology of Leiden University Medical Center and of the Georges Pompidou Hospital (HEGP, Paris) were used to evaluate the expression of DLST in a series of 85 PPGL tumors carrying germline or somatic pathogenic variants in known PPGL susceptibility genes (2 *SDHA*, 11 *SDHB*, 2 *SDHC*, 13 *SDHD*, 2 *SLC25A11*, 1 *FH*, 1 *MDH2*, 10 *VHL*,

Table 1. Further Screening by Sanger Sequencing for *DLST* Exon 14 Variants

Feature	N=169
Benign all PGL	151
Single all PGL	109
HNPGL	44
PPGL	21
PCC	43
Unknown localization	1
Multiple* PPGL	42
Multiple* HNPGL	19
Multiple* PPGL	7
Bilateral PCC	3
HNPGL + PPGL	4
PPGL + PCC	8
Unknown localization	1
Metastatic all PGL	16
Single all PGL	13
HNPGL	3
PPGL	6
PCC	4
Multiple* PPGL	3
Multiple* HNPGL	1
Bilateral PCC	1
PPGL + PCC	1
Familial PPGL	2

Main clinical and tumor features of a cohort of unexplained patients negative for other known PGL/PC-associated gene variants.
Abbreviations: HN, head and neck paraganglioma; PCC, pheochromocytoma; PGL, paraganglioma; PPGL, pheochromocytoma/paraganglioma; TAP, thoracic and abdominopelvic PPGL.
*Multiple refers to patients with more than 1 tumor at presentation.

7 *EPAS1*, 6 *NF1*, 3 *RET*, 3 *MAX*, 3 *HRAS*, and 18 without any mutation identified).

All identified patients provided written informed consent for paraganglioma genetic testing, collection of samples and subsequent analyses of LUMC samples or samples were obtained anonymously under a waiver from the institutional ethics board of the LUMC. For French patients, ethical approval for the study was obtained from the institutional review board (IRB 00003835, Comité de Protection des Personnes Ile de France IV, September 2015).

Cell culture

HEK293T cells were obtained from the ATCC (CRL-3216) and cultured in Dulbecco's Modified Eagle Medium (DMEM, Life Technologies, Paisley, UK) supplemented with 10% fetal bovine serum and penicillin/streptomycin (Life Technologies). SH-SY5Y cells were obtained from European Collection of Cell Cultures via Sigma Aldrich (St. Louis, USA, Catalog no. 86012802). SH-SY5Y cells were cultured in DMEM-F12 (Life Technologies), supplemented with 10% fetal bovine serum and penicillin/streptomycin, and maintained at 37 °C in a humidified atmosphere of 5% CO_2 in air. To rule out cell line–specific effects, most experiments were conducted in both HEK293T and SH-SY5Y cells. As these data were consistently concordant, in later experiments we chose to focus on the neuroendocrine SH-SY5Y cell line and subsequent results are based on this cell line.

DLST knockout and complementation

CRISPR-Cas9 knockout of *DLST* was carried out as described (16), with the following modifications. Single guide RNAs (sgRNA) were designed using the now retired CRISPR Design Tool (http://tools.genome-engineering.org) and all subsequent modifications were achieved using the sg*DLST*-4-F exon14, CACCGCCAGGATGGCAGACTGAGGG, and sg*DLST*-4-R exon 14, AAACCCCTCAGTCTGCCATCCTGGC sgRNAs. These sgRNAs were cloned into the pSpCas9(BB)-2A-GFP (Addgene plasmid ID: 48138) plasmid for co-expression with Cas9. Following transformation, bacterial clones (One Shot Top10 *E. coli*) were cultured, DNA isolated, and sequenced to confirm sgRNA inserts. These DNAs were then used to transfect HEK293T cells or SH-SY5Y cells using Lipofectamine 2000. Following transfection of HEK293T and SH-SY5Y, single cells were fluorescence-activated cell sorting (FACS) separated into 96-well plates containing 50% HEK293T- or SH-SY5Y-conditioned medium and 50% fresh medium to generate clonal cell lines. These clones were then cultured for 2 to 4 weeks in DMEM/10% FCS/Pen-Strep before immunocytochemical screening with an anti-DLST antibody [Abcam EPR13318(B)]. Cells with weak or negative DLST protein expression were used for isolation of genomic DNA for PCR and Sanger sequencing to identify modifications. In addition to several *DLST* knockout clones among the clones with weak/negative protein expression, we identified a HEK293T clone carrying a homozygous *DLST* p.(Pro389Leu) variant, close to the variant found in patient 1. The SH-SY5Y confirmed *DLST* knockout clones S11 and S23 were examined in detail and used in complementation experiments based on the human *DLST*-V5-6His construct (a generous gift of Dr Chris Mühlhausen (17)). This plasmid was constructed using a human DLST cDNA (GenBank accession number NM_001933.4) subcloned together with a 6His tag sequence into a pcDNA3.1/V5-His-TOPO plasmid, which is based on the standard cloning plasmid pcDNA3.1. As the V5-6His tag interfered with DLST enzyme activity (data not shown), a stop codon was introduced into the plasmid by site-directed mutagenesis using standard methods, restoring enzymatic activity to wild-type (WT) levels. The *DLST* variants c.1151C>T, p.(Pro384Leu) and c.1167C>T, p.(Pro389Leu) were then introduced into this plasmid, h*DLST*-TAG, using standard site-directed mutagenesis methods and these DNAs were then transfected into HEK293T cells or SH-SY5Y cells using Lipofectamine 2000. The confirmed DLST knockout clones S11 and S23 were examined in detail and used in complementation experiments.

Immunohistochemistry and Western blotting

Primary antibodies for immunohistochemical analysis included monoclonal mouse anti-human chromogranin A (clone DAK-A3; M0869, DAKO), polyclonal rabbit anti-S100 (Z0311; DAKO), monoclonal mouse anti-human CD56 (NCAM) (clone ERIC-1123C3; MA1-46055M7304, DAKO Invitrogen), polyclonal rabbit anti-human SDHB (HPA002868; Sigma Atlas), and monoclonal rabbit anti-DLST antibody (Rabbit mAb #11954, Cell Signaling).

Following antigen retrieval involving 10 minutes of microwave heating in Tris-EDTA buffer, pH 9.0 or citrate buffer, pH 6.0 in an autoclave at 110 °C for 5 minutes, sections were blocked for 1 hour with 10% goat serum and incubated overnight at 4 °C with primary antibodies. Signal detection was performed either with Envision+ (DAKO K3468) based on the chromogen 3,3′-diaminobenzidine or Histogreen kit (Vector Laboratories, EUROBIO/ABCYS), according to manufacturers' instructions. Immunohistochemistry images were captured using a Leica DFC550 camera, using LAS software version 4.5. Western blotting was carried out using standard methods, with the polyclonal monoclonal rabbit anti-DLST antibody [EPR13318(B); Abcam] and an anti-tubulin antibody as loading control.

Analysis of 2-oxoglutarate dehydrogenase activity

Activity of 2-oxoglutarate dehydrogenase was evaluated using a colorimetric assay kit (Catalog Number MAK189, Sigma) in cell lysates in 96-well plates. Enzyme activity was proportional to a colorimetric product with an absorbance at 450 nm (A_{450}). All samples and standards were run in duplicate. Nicotinamide adenine dinucleotide (NADH) standards were also included in the 96-well plate, with 0 (blank), 2.5, 5.0, 7.5, 10, and 12.5 nmole/well standards brought to a final volume of 50 mL with assay buffer. Cells (1 million) were washed 3 times with ice-cold phosphate-buffered saline (PBS; with CaCl2 and MgCl2) and homogenized in 100 µL ice-cold assay buffer, then further processed and assayed using the manufacturer's recommendations. Absorbance (A_{450}) was measured in a Perkin Elmer Envision microplate reader in kinetic mode for 60 minutes at 37 °C, with absorbance readings taken every minute. Absorbance at A_{450} was then calculated for each well versus time, using time points in the linear range and corrected for background by subtracting the 0 nmole NADH (blank) standard from all standards, controls, and samples. Enzyme activity was then calculated based on the generation of NADH between 2 time points encompassing the exponential phase and expressed as nmole/min/mL. In order to adjust enzyme activity for protein content, sample protein content was measured prior to analysis by standard BCA measurement (ThermoFisher Scientific/Pierce 23227 BCA Protein Assay kit) according to manufacturer's instructions.

Cell proliferation

Cell proliferation was analyzed using the xCELLigence Real-Time Cell Analysis (Roche Applied Sciences), which utilizes a gold microelectrode substrate in microtiter wells and detects impedance changes as a read-out for cell proliferation. Impedance, an inverted electrical resistance that increases as adherent-cell confluency increases, is presented as a cell index. Cell lines were seeded at a density of 20 000 cells per well in a 16-well E-Plate (Roche). The plates were loaded into the cell analysis station in the cell culture incubator immediately after seeding and measurements of the cell index were acquired every 30 minutes for 55 hours. Experiments were performed in triplicate with 6 wells/condition/experiment.

Evaluation of 5-hydroxymethyl cytosine and 5-methyl cytosine levels

Levels of 5hmC were assessed in FFPE tumor samples by immunohistochemical staining with a polyclonal rabbit antibody against 5hmC (Active Motif, AB_10013602) using standard methods as described above. Enzyme-linked immunosorbent assays (ELISA) were also used to analyze levels of 5-methyl cytosine (5mC) and 5hmC in SH-SY5Y wild-type (WT) cells and the *DLST* knockout SH-SY5Y clone S23, transfected with plasmids encoding either WT *DLST*, empty plasmid, the p.(Pro384Leu) variant or the p.(Pro389Leu) variant, using an assay previously described (18).

Statistical analysis

A Student *t* test was used to test 2-group comparisons and 1-way analysis of variance (ANOVA) was used for multigroup comparisons, with Bonferroni correction for multiple testing. The significance level was set to $P < 0.05$.

Results

Germline *DLST* variants in paraganglioma patients

We carried out exome sequencing of 5 patient samples with no known variants in genes implicated in PPGL but with phenotypic indications of possible hereditary syndromes (i.e., multiple primary tumors, tumors at a young age, or a family history of PPGL). This led to the identification of a germline heterozygous missense variant in exon 14 of the *DLST* gene, c.1151C>T, p.(Pro384Leu). Initial exome sequencing data were confirmed by Sanger sequencing, which also revealed loss of heterozygosity of the WT allele (Fig. 1). The affected patient (patient 1) was a young male who had previously developed 4 PGLs in the abdomen and thorax at the age of 23, and an additional paravertebral intrathoracic PGL that was accompanied by elevated catecholamine levels at the age of 29. There was no clear family history of PPGL, although his mother may have had a "lump" in the adrenal gland.

Following this initial identification, we performed targeted screening of *DLST* exon 14 (Table 1) in a French cohort of unexplained PPGL cases (n = 169). We identified an additional patient with a germline heterozygous variant in *DLST*, c.1121G>A, p.(Gly374Glu). This patient (patient 2) was a 71-year-old male who presented with synchronous pheochromocytoma, abdominal PGL, and thoracic PGLs. He also showed evidence of elevated noradrenaline levels. Subsequent analysis of *DLST* in tumor DNA failed to identify loss of heterozygosity around codon Gly374. However, a somatic exon 14 missense variant was identified in tumor DNA, c.1147A>G p.(Thr383Ala), indicating compound heterozygosity for these *DLST* variants (Fig. 1a). This indicates that WT *DLST* alleles were lost in both patients.

The in silico prediction algorithms Polyphen and SIFT classified the functionality of the c.1151C>T, p.(Pro384Leu) and c.1121G>A, p.(Gly374Glu) missense variants as "probably damaging" (Polyphen) and "deleterious" (SIFT), respectively. The c.1151C>T variant has been reported 4 times in 282880 alleles (allele frequency 1.41e-5) and the c.1121G>A twice in 251464 alleles (allele frequency 7.95e-6) in gnomAD. The c.1147A>G p.(Thr383Ala) variant has not been described in the gnomAD database but in silico analyses indicated that the variant is likely pathogenic.

We then assessed the conservation of the 3 variants using the OMA database, which provides alignments of very large numbers of orthologs (Fig. 1b). All 3 variants [p.(Pro384Leu), p.(Gly374Glu), and p.(Thr383Ala)] are highly conserved to the bacterial level. We then considered the likely impact of the variants on protein structure. All variants affect the same, highly conserved, structure in a substrate binding pocket of the catalytic domain, and as such likely interfere with catalytic function (Fig. 1c). In Fig. 2 we provide an overview of all currently known *DLST* variants in PPGL cases (N = 8), including those found by Remacha et al (13).

Histopathological analysis of *DLST*-mutated paragangliomas

The (immuno)histochemical appearance of FFPE tumor samples from patient 1 was characteristic of paraganglioma, but with a slightly less prominent "cell nest" morphology than found in many other paragangliomas (Fig. 3a-3c). The tumor was positive for chromogranin A and synaptophysin (not shown), together with S100, CD56 (NCAM), and SDHB (Fig. 3d-f). SDHB staining was homogenous, but S100 and CD56 showed a heterogeneous pattern, with S100 exhibiting a pattern of diffuse cytoplasmic staining in the majority of tumor cells, but with areas showing the more typical pattern of negative chromaffin cells and intensely staining sustentacular cells (Fig. 3d).

Staining for DLST was assessed by immunohistochemistry in 2 PPGL tumors of patient #1 and 1 of patient #2 and compared to a series of 85 PPGL tumor samples carrying mutations in the different PPGL susceptibility genes (Table 2). Interestingly, as previously described by Remacha et al, we observed a strong cytosolic and sometimes patchy staining in all 3 *DLST*-mutated tumors, as well as in most of TCA-cycle–mutated tumors (26/28 *SDHx*, 1/1 *FH*, 1/2 *SLC25A11*) (Table 2, Fig. 4) while the staining was less intense and showed the typical aspect of a granular mitochondrial localization in most cluster 2, *VHL*, and *EPAS1*-mutated tumors.

Functional studies of *DLST* variants in vitro

To determine whether *DLST* variants might result in a loss of functional activity, we chose to examine the patient 1 variant c.1151C>T, p.(Pro384Leu) in detail. We first generated knockouts of *DLST* in the HEK293T (data not shown) and neuroblastoma SH-SY5Y cell lines using CRISPR-Cas9 single guide RNAs (sgRNA) designed to induce disruptive mutations in exon 14 of *DLST*, which is highly conserved and is also the site of all variants identified in this study. Knockouts of *DLST* were identified by immunocytochemical screening with anti-*DLST* (Fig. 5a and 5b) and subsequently confirmed in detail by PCR and Sanger sequencing of genomic DNA from clones to identify exact modifications (Fig. 5c and 5d) and by Western blotting to confirm loss of protein expression (Fig. 5e). In addition to several homozygous *DLST*-negative knockout clones, we serendipitously identified a clone carrying a homozygous c.1167C>T, p.(Pro389Leu) missense variant. This variant affected a highly conserved amino acid close to the patient variant under study (Fig. 1b). As shown by immunocytochemistry (Fig. 6a) and Western blot (Fig. 6b) using anti-DLST, the protein expression of DLST was approximately equivalent in the various clones.

Activity of 2-oxoglutarate dehydrogenase was initially evaluated in HEK293T cells (data not shown). We then evaluated enzyme activity in SH-SY5Y WT cells and the SH-SY5Y *DLST* null clone S23, transfected with plasmids encoding either WT *DLST*, empty plasmid (EP), the p.(Pro384Leu) variant (P384L), or the p.(Pro389Leu) variant (P389L). A representative assay (Fig. 6c) illustrates the relative levels of enzyme activity for the p.(Pro384Leu) and p.(Pro389Leu) variants compared to the native cell line and the S23 null clone transfected with WT *DLST* or empty plasmid. DLST knockout dramatically effects 2-oxoglutarate dehydrogenase enzyme activity, which is fully rescued upon reintroduction of a WT *DLST* cDNA construct. Quantification of 2 independent assays conducted in duplicate in the S23 clone (Fig. 6d) indicated that, compared to the S23 clone transfected with WT *DLST*, the p.(Pro384Leu) and p.(Pro389Leu) variants showed 17% and 5% of normal activity, respectively (*both $P < 0.0001$ versus S23 + WT).

Real-time cell proliferation was analyzed in native SH-SY5Y cells and in SH-SY5Y null clone S23, transfected with plasmids encoding either WT *DLST*, the p.(Pro384Leu) variant, or empty plasmid. Although less pronounced than the changes evident in enzyme activity, the clone carrying the p.(Pro384Leu) patient variant showed a clear decrease in cell proliferation (Fig. 6e; representative assay) compared with native SH-SY5Y cells or the S23 WT *DLST* clone.

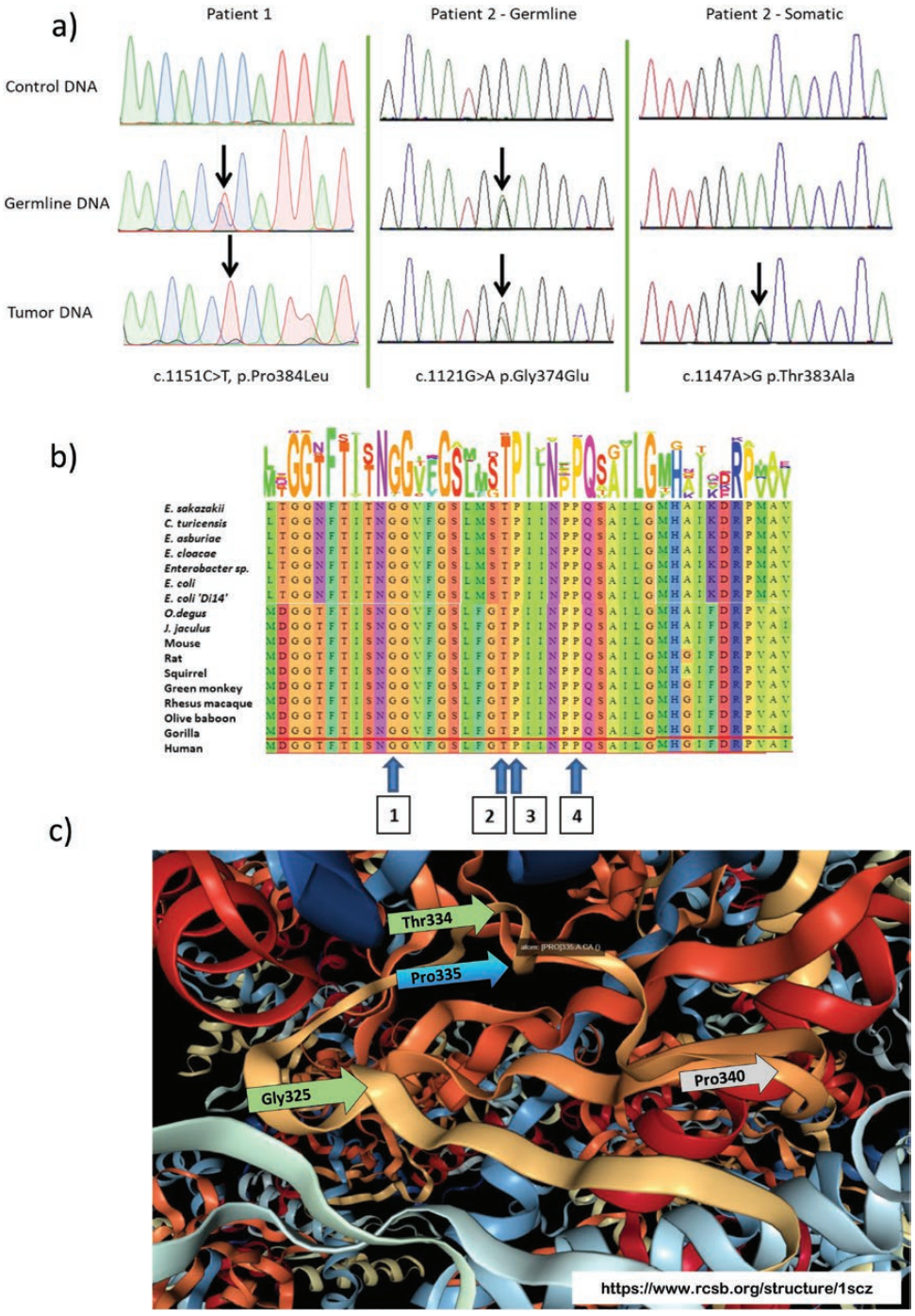

Figure 1. The dihydrolipoamide succinyltransferase gene variants identified in patients in this study. a) DNA analysis of the patient variants identified in this study. Patient 1 carried an exon 14 variant, c.1151C>T, p.(Pro384Leu). This variant was heterozygous in germline DNA, with loss of heterozygosity (LOH) in tumor DNA. Patient 2 carried a heterozygous exon 14 variant, c.1121G>A, p.(Gly374Glu), but showed no evidence of LOH in tumor DNA. Analysis of tumor DNA from this patient identified a second, somatic variant only present in tumor DNA, c.1147A>G, p.(Thr383Ala), indicating that this patient carried compound heterozygous variants in germline and somatic DNA. b) Amino acid conservation of exon 14 dihydrolipoamide succinyltransferase (DLST) variants found in this study, 1) c.1121G>A, p.(Gly374Glu); 2) c.1147A>G, p.(Thr383Ala); 3) c.1151C>T, p.(Pro384Leu); 4) c.1167C>T, p.(Pro389Leu—experimental variant identified in the course of the present study), visualized in the OMA (Orthologous MAtrix project browser; https://omabrowser.org/). Letter height and number of letters approximates to level of conservation in an orthologous group of proteins, in this case OMA Group 774252 that includes 43 archaea, 966 bacteria and 297 eukaryotes. All variants are highly conserved. c) Structural model of *E.coli* dihydrolipoamide succinyltransferase (RCSB Protein Data Bank 1E2O, "catalytic domain from dihydrolipoamide succinyltransferase," deposited by Knapp et al (20)), illustrating that the variants described in this study are all located in the binding pocket for the S-succinyldihydrolipoyl moiety within the catalytic domain. The mixed ribbon/ball-and-stick cartoon shows the locations of c.1121G>A, p.(Gly374Glu) (*H.sapiens*) = p.Gly325 (*E.coli*); c.1147A>G p.(Thr383Ala) (*H.sapiens*) = p.Thr334 (*E.coli*); c.1151C>T, p.(Pro384Leu) (*H.sapiens*) = p.Pro335 (*E.coli*); and the experimental variant identified in the course of the present study, c.1167C>T, p.(Pro389Leu) (*H.sapiens*) = p.Pro340 (*E.coli*), with arrows indicating the equivalent *H. sapiens* residues.

Figure 2. Currently known PPGL patient variants in the dihydrolipoamide succinyltransferase gene. Alignment of dihydrolipoamide succinyltransferase (DLST) protein sequences of *Homo sapiens* and *Escherichia coli* (https://www.bioinformatics.nl/cgi-bin/emboss/showalign), with highly conserved sequences highlighted in light green. Variants found in this study are indicated by black (patient) and red (experimental) arrows: 1) c.1151C>T, p.(Pro384Leu); 2) c.1147A>G, p.(Thr383Ala); 3) c.1121G>A, p.(Gly374Glu); 4) c.1167C>T, p.(Pro389Leu), experimental variant. Variants identified by Remacha et al. are indicated by blue (pathogenic) or green (SNP or VUS) arrows: 5) c.692G>A, p.Arg231Gln; 6) c.910G>A, p.Asp304Asn (likely SNP); 7) c.1121G>A, p.(Gly374Glu); 8) c.1265A>G, p.Tyr422Cys (VUS, based on functional analysis by Remacha et al).

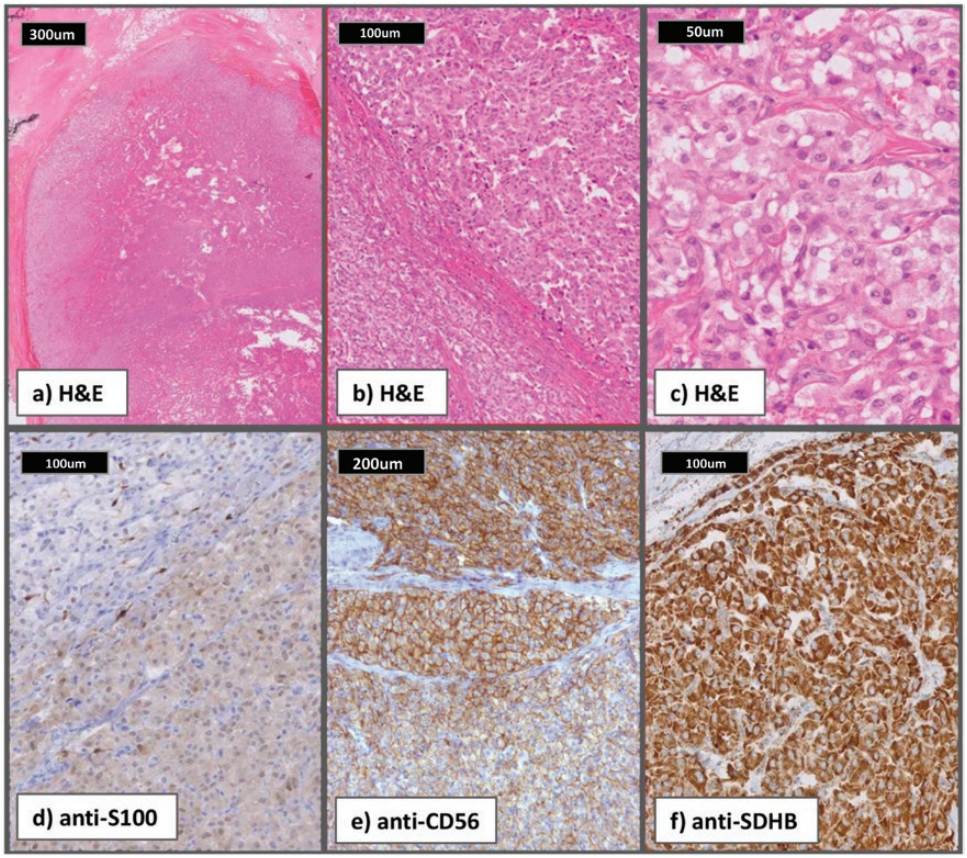

Figure 3. Representative (immuno)histochemical staining of an FFPE tumor from patient 1 carrying the DLST p.(Pro384Leu) variant. a) Hematoxylin and eosin (H&E) (5× objective), b) H&E (20× obj.), c) H&E (40× obj.). Staining for d) S100 (20× obj.) and e) CD56 (NCAM) (10× obj.) was relatively heterogeneous. The tumor was positive for f) SDHB (20× obj.). Scale bars indicate respective sizes.

Table 2. DLST Immunostaining in PPGL Samples With Various Types of PPGL Susceptibility Gene Variants Reveals Non-Mitochondrial Cytosolic Staining in all DLST-Mutated Cases and Most TCA-Cycle–Related Tumors

	DLST immunostaining	
Gene mutated	Cytosolic/patchy	Mitochondrial granular
DLST (n = 3)	3	
SDHA (n = 2)	1	1
SDHB (n = 11)	10	1
SDHC (n = 2)	2	
SDHD (n = 13)	13	
SLC25A11 (n = 2)	1	1
FH (n = 1)	1	
MDH2 (n = 1)		1
VHL (n = 10)	1	9
EPAS1 (n = 7)	2	5
NF1 (n = 6)	3	3
RET (n = 3)		3
MAX (n = 3)		3
HRAS (n = 3)		3
Not mutated (n = 18)	4	14
TOTAL	**41**	**44**

Epigenetic changes

Loss-of-function mutations in TCA cycle enzymes such as succinate dehydrogenase (SDH) or fumarate hydratase (FH) are known to cause inhibition of numerous oxoglutarate-dependent dioxygenases, including histone demethylases and the TET family of 5-methylcytosine hydroxylases (7, 8, 10, 19). To evaluate the impact of *DLST* variants on DNA methylation, we analyzed the levels of 5hmC using immunohistochemistry in FFPE tissue samples. We observed that, compared with normal human carotid body (Fig. 7a) and a non-SDH PGL (Fig. 7b), *DLST*-mutated tumors (Fig. 7c and 7d) showed lower levels of 5hmC, levels that were similar to those observed in an *SDHB*-mutated PGL (Fig. 7e) or an *SDHD*-mutated carotid body PGL (Fig. 7f). Low 5hmC was observed in all tumor tissues studied (2 from patient #1 and one from patient #2 [data not shown]). DNA methylation and hydroxymethylation were also assessed in SH-SY5Y S23 clones using ELISA. This analysis revealed a significant increase in 5mC in clones carrying the p.(Pro384Leu) variant or the p.(Pro389Leu) variant compared with control cells ($P < 0.01$) (Fig. 7g). By contrast, 5hmC levels were reduced ($P < 0.01$ versus SH-SY5Y and S23 + WT) compared with the native cell line and the WT plasmid-transfected S23 clone (Fig. 7h).

Discussion

In this study, we investigated 3 likely pathogenic variants of *DLST*, the gene that encodes dihydrolipoamide S-succinyltransferase, the E2 subunit of the 2-oxoglutarate dehydrogenase enzyme complex. This enzyme complex catalyzes the transfer of the succinyl group from an S-succinyldihydrolipoyl moiety to coenzyme A as part of the overall conversion of 2-oxoglutarate to succinyl-CoA and CO_2 by 2-oxoglutarate dehydrogenase. Recently,

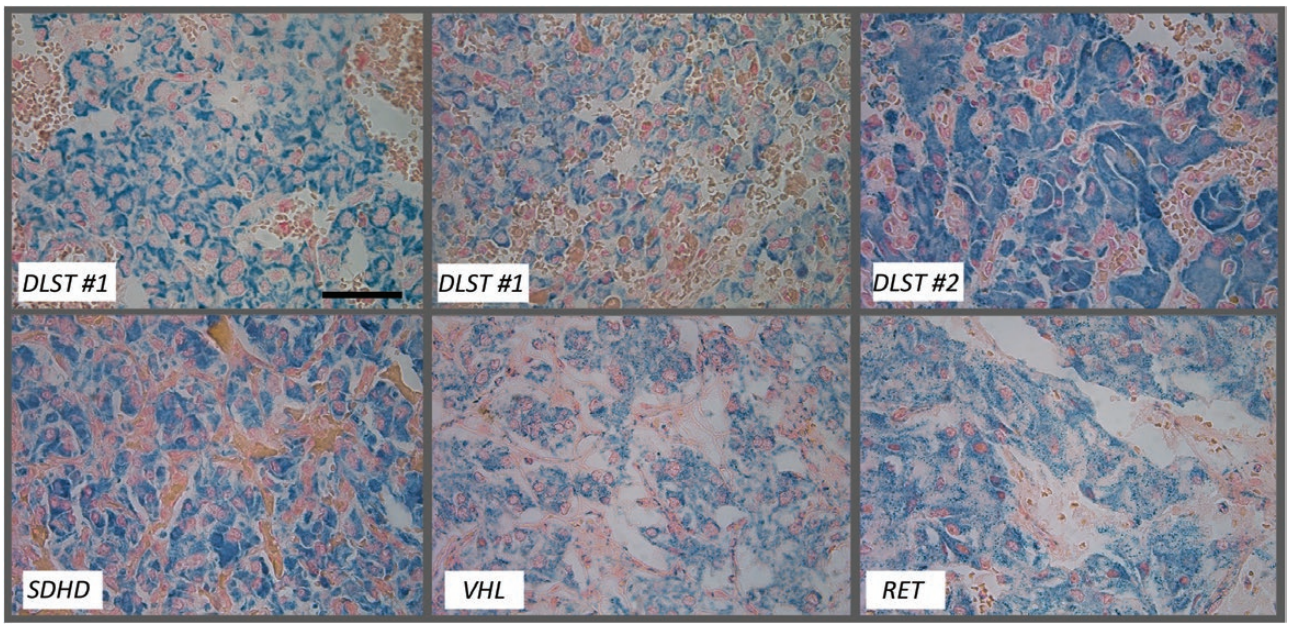

Figure 4. Analysis of DLST immunostaining in PPGL tumors. Immunohistochemical analysis shows positive labeling of cytoplasmic aggregates in *DLST*-mutated tumors from patient #1 and #2 and in an *SDHD*-mutated PGL, compared with a *VHL* and a *RET*-mutated tumor that show mitochondrial staining. Scale bar = 50μm.

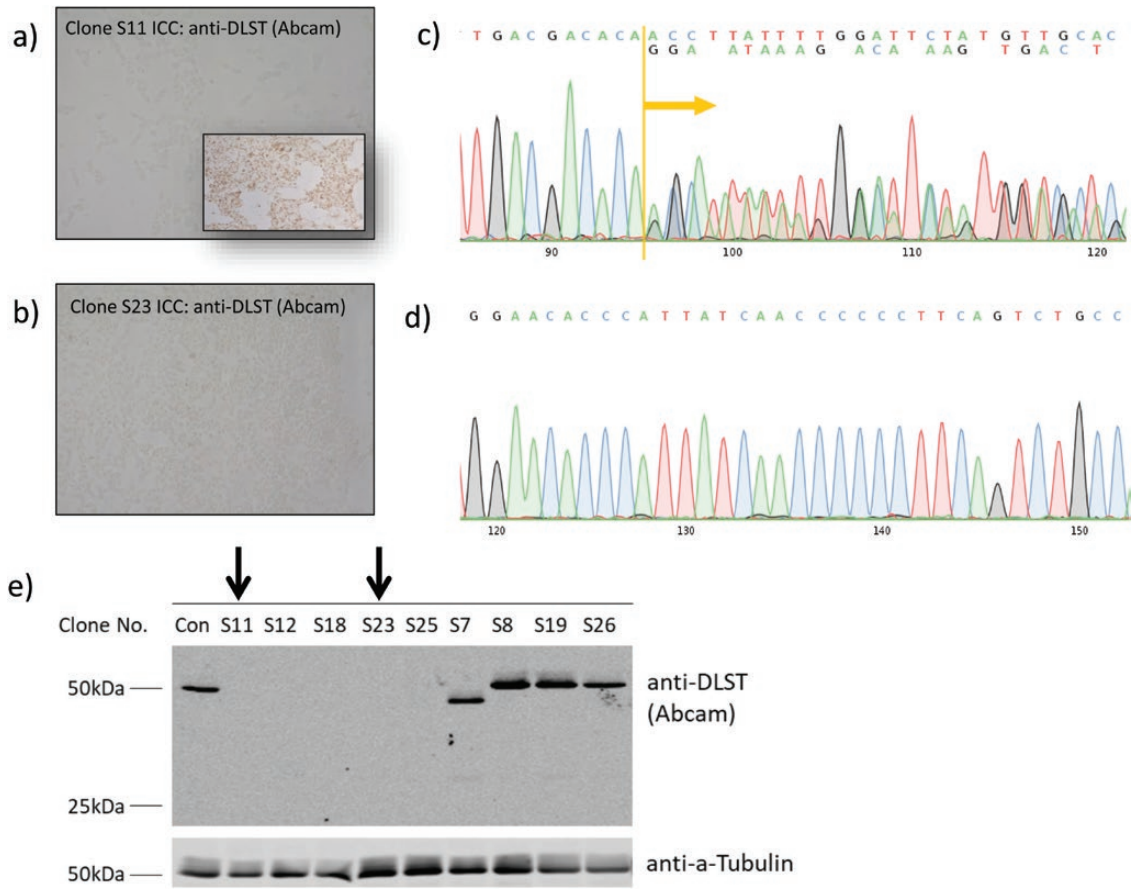

Figure 5. Verification of DLST knockout in CRISPR-Cas9 targeted SH-SY5Y clonal cell lines. a) Clone S11 carried variants in both allele 1, a 20bp deletion, and in allele 2, a 10bp deletion upon Sanger sequencing. Disambiguation of this compound knockout showed allele 1 to result in a frameshift from position 305 of the protein, resulting in a truncated 308–amino acid protein, while allele 2 resulted in a frameshift from position 307, leading to a truncated 334–amino acid protein. b) Immunocytochemistry confirmed loss of DLST protein expression in the S11 clone, compared with wild-type SH-SY5Y cells (inset). c) Clone S23 showed a homozygous 1bp insertion in both alleles, resulting in a frameshift from position 389 of the protein and a truncated 400–amino acid protein. d) Immunocytochemistry confirmed loss of DLST protein expression in clone S23. e) Western blot of protein extracts from a series of CRISPR-Cas9-targeted clones, followed by immunoblotting with anti-DLST antibody or anti-tubulin as a loading control confirmed complete loss of protein expression in the 2 clones described here (arrows).

Remacha et al reported germline variants in *DLST* in 8 patients with PPGL (13). As an important component of 2-oxoglutarate dehydrogenase, the rate-limiting enzyme of the TCA cycle, PPGL-associated variants in *DLST* constitute a further link between PPGL and energy metabolism previously established by the identification of the *SDHx, IDHx, FH, MDH2, SLC25A11*, and *GOT2* genes.

We showed that the p.(Pro384Leu) variant, located in the catalytic site of *DLST*, leads to a dramatic but not complete loss of catalytic activity. Although we did not have an opportunity to assess the catalytic activity of p.(Gly374Glu) or p.(Thr383Ala), their location proximal to p.(Pro384Leu) strongly suggests that they will affect catalytic activity. In the case of p.(Gly374Glu), this assumption is supported by evidence reported by Remacha et al in which this variant was linked to an increased 2-oxoglutarate-to-fumarate ratio and the buildup of the metabolite 2-hydroxyglurate in p.(Gly374Glu)-mutated tumors, supporting the assumption that this variant disrupts OGDH complex activity. These authors also reported a highly conserved *DLST* variant, c.1265A>G, p.(Tyr422Cys), for which a predicted deleterious effect in silico could not be validated by in vitro studies.

A characteristic of variants in many PPGL-associated metabolic genes is the accumulation of intermediate metabolites such as succinate or fumarate, which may act as oncometabolites by inhibiting 2OG-dependent dioxygenases. Among 2OG-dependent enzymes, TET enzymes are involved in controlling the demethylation of DNA by hydroxylating 5mC to 5hmC. Knockout of succinate dehydrogenase or addition of exogeneous succinate has been shown to inhibit JmjC-domain-containing histone demethylases (JHDM) in yeast and

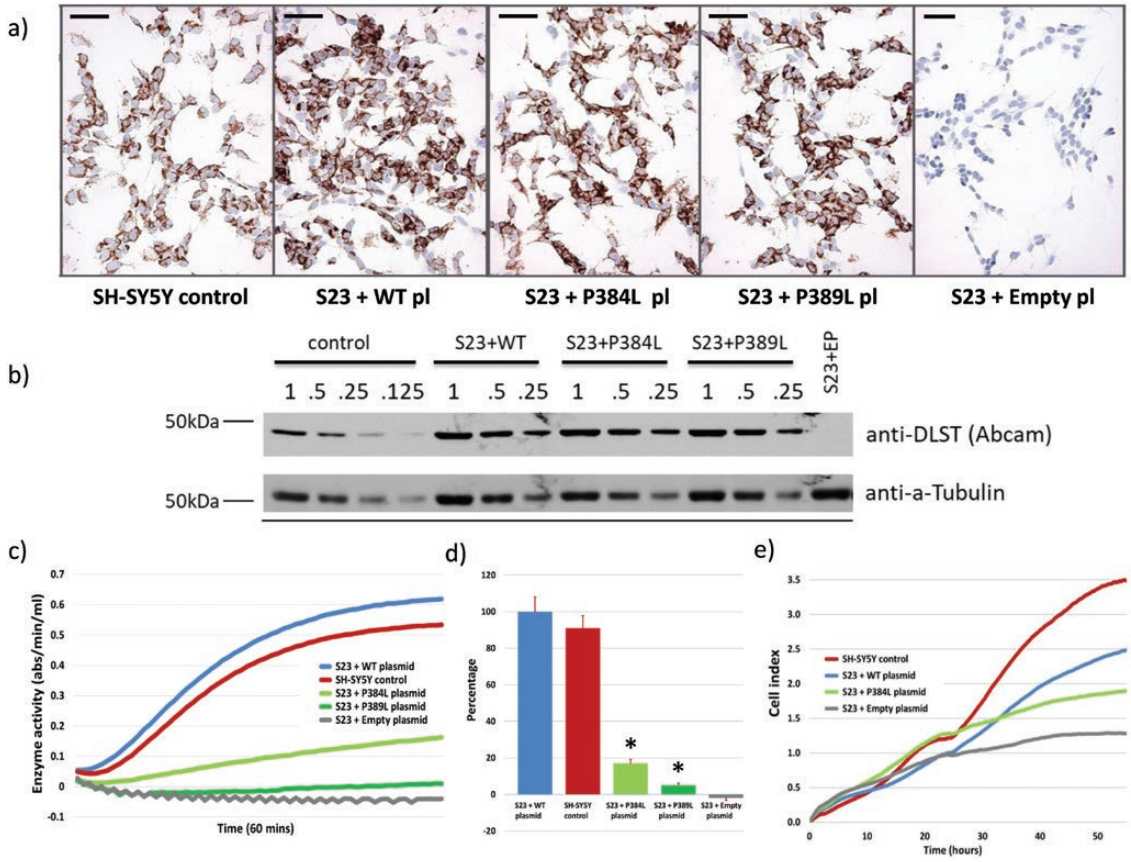

Figure 6. Crispr-Cas9-mediated knockout of DLST variants results in loss of enzyme activity and reduce proliferation. a) As determined by immunocytochemical staining, the p.(Pro384Leu) and p.(Pro389Leu) clones showed levels of DLST protein expression comparable to WT DLST-transduced knockout clone S23 or WT SH-SY5Y cells. Scale bars (50um) are shown. b) Western blot of a dilution series of protein extracts from the various clonal cell lines, followed by immunoblotting with anti-DLST antibody or anti-tubulin as a loading control, illustrating that amounts of DLST were approximately equivalent between cell lines. c) Representative 2-oxoglutarate dehydrogenase enzyme activity in the SH-SY5Y parental cell line and the *DLST* knockout clone S23 complemented with either WT *DLST*, p.(Pro384Leu), p.(Pro389Leu) or empty plasmid. d) The p.(Pro384Leu) and p.(Pro389Leu) clones showed 17% and 5% enzyme activity (*$P < 0.0001$ versus SH-SY5Y and S23 + WT), respectively, compared with the SH-SY5Y parental cell line. e) Cell proliferation analyzed in the xCELLigence Real-Time cell analysis system (averaged cell index, n = 6). Cell lines were seeded at a density of 20 000 cells per well and impedance measurements were acquired every 30 minutes for 55 hours. Experiments were performed in triplicate.

humans (7, 8), and TET enzymes (19), leading to histone and genome-wide DNA hypermethylation, respectively (9, 10). Methylation data on *DLST* tumors reported by Remacha et al classified them in the intermediate M2 cluster, which lies between the hypermethylated CpG-island methylator-phenotype (CIMP) and hypomethylated clusters. We showed here that *DLST* variants lower 5hmC levels in patient tumors (Fig. 7c and 7d) and alter the levels of 5hmC and 5mC in a cell system, decreasing 5hmC while increasing 5mC (Fig. 7h and 7g, respectively). This indicates that accumulation of 2-oxoglutarate and/or 2-hydroxyglutarate is likely influencing the activity of TET enzymes, thereby promoting DNA hypermethylation.

None of the patients in this study showed a clear family history of disease, a characteristic similar to the individuals identified by Remacha et al. In addition, 7 of the 8 individuals described by these authors had tumors in multiple locations, particularly in the thorax or abdomen, a phenotype identical to the 2 additional individuals described here. As such, *DLST* patients seem to more closely resemble *SDHB* than *SDHD*-linked patients. Interestingly, a non-mitochondrial DLST staining was observed in all DLST-mutated tumors, as well as in SDH-deficient PPGL, suggesting that TCA-cycle–related tumors may share a similar improper localization of the DLST protein.

In conclusion, we describe likely pathogenic variants in *DLST*, a subunit of the ODGH complex, which appear to predispose to PPGLs with a predominantly abdominal-thoracic presentation and an occurrence in families that resembles the often sporadic-like presentation of *SDHB*, predicting that *DLST* will show low penetrance once sufficient cases become available for analysis.

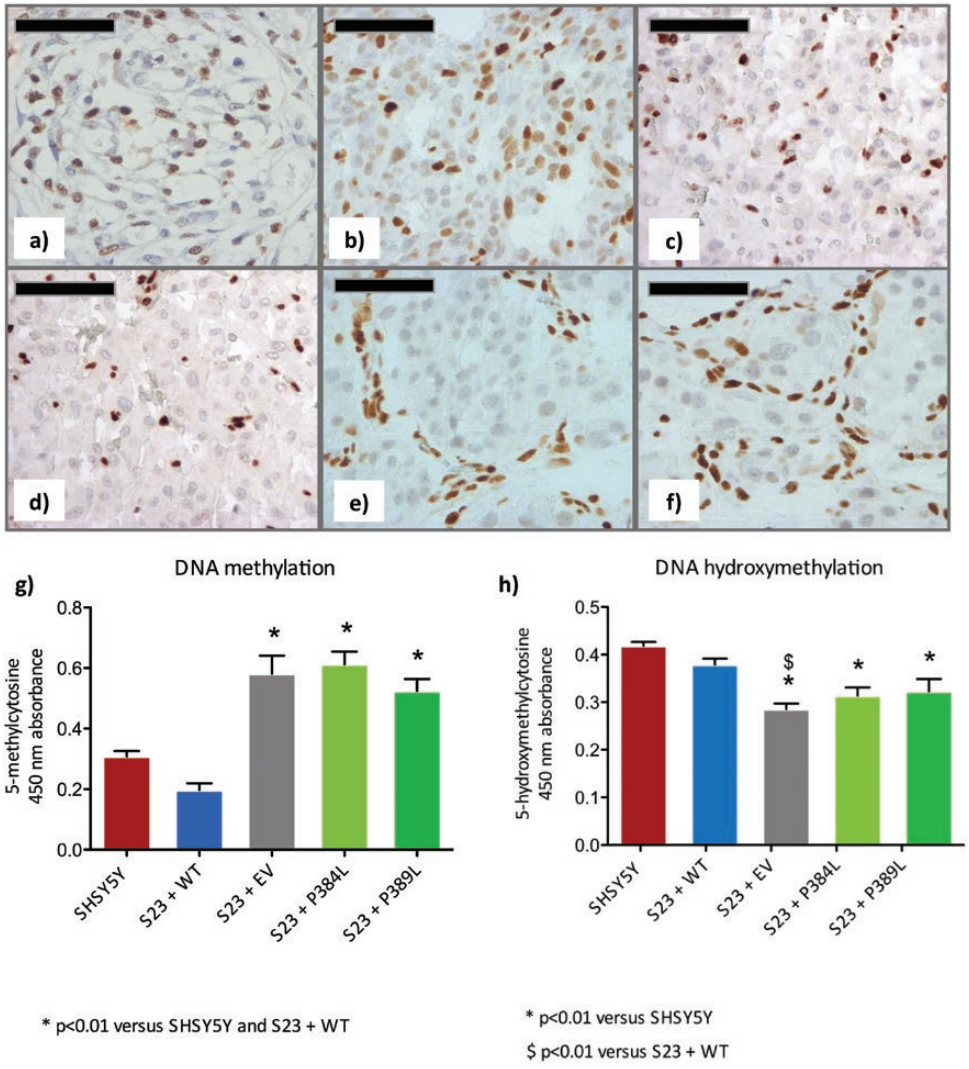

Figure 7. DLST variants result in epigenetic changes in FFPE patient samples and cell clones. Immunohistochemical staining of 5hmC in a) normal human carotid body and b) SDH WT paraganglioma, shows nuclear staining in both tumor and stromal cells, while in c) *DLST*-mutated paraganglioma (p.P384L-tumor 1), d) *DLST*-mutated paraganglioma (p.P384L-tumor 2), e) *SDHB*-mutated paraganglioma and f) *SDHD*-mutated carotid body paraganglioma, the staining is restricted to stromal cells, but mostly absent in the nuclei or tumor cells. Scale bar indicates 50 µm. Analysis of methylation using 5-methyl cytosine (5mC) and 5-hydroxymethyl cytosine (5hmC) enzyme-linked immunosorbent assays (ELISA). SH-SY5Y WT cells and the DLST knockout SH-SY5Y clone S23, transfected with plasmids encoding either WT DLST (WT), empty plasmid (EP), the p.(Pro384Leu) variant, or the p.(Pro389Leu) variant, were assessed for levels of g) 5mC (* $P < 0.01$ versus SH-SY5Y and S23 + WT) and h) 5hmC (* $P < 0.01$ versus SH-SY5Y, $ $P < 0.01$ versus S23 + WT).

Acknowledgments

We would like to thank Dr Chris Mühlhausen for providing the DLST construct, Ing Dominique Duesman for immunohistochemical stainings, Dr Eline van Meel and Professor Hans Aerts for help with setting up enzyme activity assays, and Ing Jaap van Eendenburg for support with the xCELLigence assay.

Financial Support: This work was supported by the Dutch Cancer Society (Grant 2011–5025 to JPB/PD) and by the Ligue Nationale contre le Cancer (Equipe Labellisée, to AB/APGR/JF) and the Institut National du Cancer and the Direction Générale de l'Offre de Soins (PRT-K 2014, COMETE-TACTIC, INCa-DGOS_8663). A. Buffet received financial support from ITMO Cancer AVIESAN (Alliance Nationale pour les Sciences de la Vie et de la Santé, National Alliance for Life Sciences & Health) within the framework of the Cancer Plan and from la Fondation pour la Recherche Médicale (FDT20170436955). We thank the Biological Resources Center and Tumor Bank Platform, Hôpital Européen Georges Pompidou (BB-0033-00063) and Justine Woszczyk for technical assistance.

Additional Information

Correspondence and Reprint Requests: Jean-Pierre Bayley, PhD, Department of Human Genetics, Leiden University Medical Centre, Albinusdreef 2, 2333 ZA Leiden, The Netherlands. E-mail: j.p.l.bayley@lumc.nl.

Disclosure Summary: The authors have no conflicts of interest to disclose.

Data Availability: Some or all data generated or analyzed during this study are included in this published article or available from the authors on reasonable request.

References

1. Lack E. *Atlas of Tumor Pathology: Tumors of the Adrenal Gland and Extra-Adrenal Paraganglia*. AFIP Fasicle No. 19. ed. Washington DC: American Registry of Pathology; 1997.
2. Neumann HPH, Young WF Jr, Eng C. Pheochromocytoma and Paraganglioma. *N Engl J Med*. 2019;**381**(6):552-565.
3. Fishbein L. Pheochromocytoma/Paraganglioma: is this a genetic disorder? *Curr Cardiol Rep*. 2019;**21**(9):104.
4. Pollard PJ, Brière JJ, Alam NA, et al. Accumulation of Krebs cycle intermediates and over-expression of HIF1alpha in tumours which result from germline FH and SDH mutations. *Hum Mol Genet*. 2005;**14**(15):2231-2239.
5. Selak MA, Armour SM, MacKenzie ED, et al. Succinate links TCA cycle dysfunction to oncogenesis by inhibiting HIF-alpha prolyl hydroxylase. *Cancer Cell*. 2005;**7**(1):77-85.
6. Xu W, Yang H, Liu Y, et al. Oncometabolite 2-hydroxyglutarate is a competitive inhibitor of α-ketoglutarate-dependent dioxygenases. *Cancer Cell*. 2011;**19**(1):17-30.
7. Smith EH, Janknecht R, Maher LJ 3rd. Succinate inhibition of alpha-ketoglutarate-dependent enzymes in a yeast model of paraganglioma. *Hum Mol Genet*. 2007;**16**(24):3136-3148.
8. Cervera AM, Bayley JP, Devilee P, McCreath KJ. Inhibition of succinate dehydrogenase dysregulates histone modification in mammalian cells. *Mol Cancer*. 2009;**8**:89.
9. Hoekstra AS, de Graaff MA, Briaire-de Bruijn IH, et al. Inactivation of SDH and FH cause loss of 5hmC and increased H3K9me3 in paraganglioma/pheochromocytoma and smooth muscle tumors. *Oncotarget*. 2015;**6**(36):38777-38788.
10. Letouzé E, Martinelli C, Loriot C, et al. SDH mutations establish a hypermethylator phenotype in paraganglioma. *Cancer Cell*. 2013;**23**(6):739-752.
11. Dahia PL, Ross KN, Wright ME, et al. A HIF1alpha regulatory loop links hypoxia and mitochondrial signals in pheochromocytomas. *Plos Genet*. 2005;**1**(1):72-80.
12. Fishbein L, Leshchiner I, Walter V, et al.; Cancer Genome Atlas Research Network. Comprehensive molecular characterization of pheochromocytoma and paraganglioma. *Cancer Cell*. 2017;**31**(2):181-193.
13. Remacha L, Pirman D, Mahoney CE, et al. Recurrent Germline DLST mutations in individuals with multiple pheochromocytomas and paragangliomas. *Am J Hum Genet*. 2019;**104**(5):1008-1010.
14. Lenders JW, Duh QY, Eisenhofer G, et al.; Endocrine Society. Pheochromocytoma and paraganglioma: an endocrine society clinical practice guideline. *J Clin Endocrinol Metab*. 2014;**99**(6):1915-1942.
15. N.G.S._PPGL_Study_Group, Toledo RA, Burnichon N, et al. Consensus Statement on next-generation-sequencing-based diagnostic testing of hereditary phaeochromocytomas and paragangliomas. *Nat Rev Endocrinol*. 2017;**13**(4):233-247.
16. Ran FA, Hsu PD, Wright J, Agarwala V, Scott DA, Zhang F. Genome engineering using the CRISPR-Cas9 system. *Nat Protoc*. 2013;**8**(11):2281-2308.
17. Schmiesing J, Schlüter H, Ullrich K, Braulke T, Mühlhausen C. Interaction of glutaric aciduria type 1-related glutaryl-CoA dehydrogenase with mitochondrial matrix proteins. *Plos One*. 2014;**9**(2):e87715.
18. Buffet A, Morin A, Castro-Vega LJ, et al. Germline mutations in the mitochondrial 2-Oxoglutarate/Malate carrier SLC25A11 gene confer a predisposition to metastatic paragangliomas. *Cancer Res*. 2018;**78**(8):1914-1922.
19. Xiao M, Yang H, Xu W, et al. Inhibition of α-KG-dependent histone and DNA demethylases by fumarate and succinate that are accumulated in mutations of FH and SDH tumor suppressors. *Genes Dev*. 2012;**26**(12):1326-1338.
20. Knapp JE, Mitchell DT, Yazdi MA, Ernst SR, Reed LJ, Hackert ML. Crystal structure of the truncated cubic core component of the Escherichia coli 2-oxoglutarate dehydrogenase multienzyme complex. *J Mol Biol*. 1998;**280**(4):655-668.